Available online at www.sciencedirect.com

ScienceDirect

IFAC PapersOnline CONFERENCE PAPER ARCHIVE

IFAC PapersOnLine 58-27 (2024) 67–72

Reduction to spectral submanifolds in guided car-following with time delay

Bence Szaksz *, **Gábor Orosz** **, and **Gabor Stepan** *

* *Department of Applied Mechanics, Faculty of Mechanical Engineering, Budapest University of Technology and Economics, Budapest, H-1111, Hungary (e-mail: szaksz@mm.bme.hu, stepan@mm.bme.hu).*

** *Department of Mechanical Engineering, and Department of Civil and Environmental Engineering, University of Michigan, Ann Arbor, MI 48109, USA (e-mail: orosz@umich.edu)*

Abstract: The reduced order dynamics of a car-following model is investigated when an automated lead vehicle provides guidance to a human driver. Considering the relevant time delay, the system dynamics is governed by a delay differential equation, which has an infinite dimensional spectrum. In order to carry out model reduction, the concept of spectral submanifolds is extended to time delay systems. The dynamics is projected from the infinite dimensional state space to a low-dimensional invariant manifold. The spectral submanifold calculation is carried out both for a real dominant eigenvalue and for a pair of complex conjugate dominant eigenvalues to extract the essential nonlinear dynamics.

Keywords: Systems with time-delays, Infinite-dimensional systems, Nonlinear model reduction, Automated vehicles, Human and vehicle interaction

1. INTRODUCTION

In the coming years, mixed traffic flows of automated vehicles (AVs) and human-driven vehicles (HVs) are expected to travel on highways (Molnar and Orosz, 2024). In these car-following situations, AVs with appropriately tuned control can reduce fuel consumption and improve safety not only for themselves but also for nearby HVs. The human reaction time and nonlinear behavior are governed by nonlinear delay differential equations, which have infinite-dimensional state space representation (Stepan, 1989). Therefore, considering relevant nonlinearities in the dynamics, advanced model reduction techniques are needed for the control design of AVs mixed in traffic.

Spectral decomposition is a powerful tool for the analysis of linear dynamical systems, however, it cannot be applied in the presence of essential nonlinearities. Nonlinear normal modes were first introduced as the synchronous periodic oscillations of conservative systems (Rosenberg, 1966). This concept was generalized for dissipative systems at the end of the 20th century by Shaw and Pierre (1993). They defined nonlinear normal modes as invariant manifolds, which are tangent to the space spanned by the eigenvectors of the linearized system. However, the surfaces corresponding to the normal modes are not unique (Cirillo et al., 2016). The unique smoothest nonlinear continuation of the spectral subspace of the linearized system was introduced by Haller and Ponsioen (2016); they called this surface spectral submanifold (SSM). In the last years, several papers applied this model reduction technique both for autonomous and for non-autonomous dynamical systems (Szalai et al., 2017; Breunung and Haller, 2018; Vizzaccaro et al., 2021; Cenedese et al., 2022; Opreni et al., 2023).

Here, we extend the concept of SSM for time delay systems with the help of the dual perturbation framework, also called sun-star calculus (Diekmann et al., 1995; Wage, 2014; Lentjes et al., 2023). The simplest car-following model is considered when an AV is traveling in front of an HV. The SSM together with the corresponding reduced dynamics are obtained both for a dominant real eigenvalue and for a dominant pair of complex conjugate eigenvalues of the linearized system. The obtained reduced models extract the essential finite-dimensional dynamics of the infinite-dimensional system supporting the control design in mixed car-following scenarios.

2. PROBLEM STATEMENT

Assume that an automated vehicle (AV) is driving in front of a human-driven vehicle (HV) in a distance of h_{-1}, while the velocities of the AV and HV are v and v_{-1}, respectively; see Fig. 1(a). We consider that the human driver takes into account the standard range policy function $V(h_{-1})$; see Fig. 1(b) and the velocity difference between the two vehicles with the gains α and β, respectively. Furthermore, the control of the AV is also based on two terms: the gain $\hat{\beta}$ relates to the AV velocity deviation with respect to the reference velocity v_{ref}, while the gain

⋆ The work of BSz was partially supported by the MTA-BME Lendulet "Momentum" Global Dynamics Research Group, Budapest, Hungary, while the work of GS was partially supported by the HUN-REN–BME Dynamics of Machines Research Group, Budapest, Hungary. GO acknowledges the support of the Hungarian Academy of Sciences within the Distinguished Guest Fellowship Programme and the support of the Fulbright Foundation.

10.1016/j.ifacol.2024.10.301

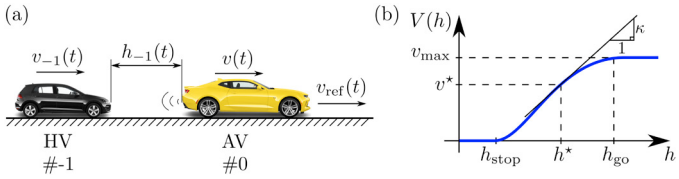

Fig. 1. (a) car-following model; (b) the nonlinear range policy of the human driver.

β_{-1} corresponds to the velocity difference between the two cars. The corresponding governing equations are

$$\dot{h}_{-1}(t) = v(t) - v_{-1}(t)\,, \tag{1}$$

$$\begin{aligned}\dot{v}_{-1}(t) =& \alpha(V(h_{-1}(t-\tau)) - v_{-1}(t-\tau)) \\ &+ \beta(v(t-\tau) - v_{-1}(t-\tau))\,,\end{aligned} \tag{2}$$

$$\begin{aligned}\dot{v}(t) =& \hat{\beta}(v_{\mathrm{ref}} - v(t-\tau)) \\ &+ \beta_{-1}(v_{-1}(t-\tau) - v(t-\tau))\,,\end{aligned} \tag{3}$$

where, for the sake of simplicity, the same time delay τ is assumed in the control loop of the HV and the AV. Similar car following models were analysed in Szaksz et al. (2023) and Szaksz et al. (2024).

According to Molnar and Orosz (2024), the headway-based range policy function assumes the form

$$V(h) = \begin{cases} 0, & \text{if } h < h_{\mathrm{stop}}\,, \\ F(h), & \text{if } h_{\mathrm{stop}} \le h < h_{\mathrm{go}}\,, \\ v_{\max}, & \text{if } h_{\mathrm{go}} \le h\,, \end{cases} \tag{4}$$

where $F(h)$ is the third degree polynomial

$$F(h) = v_{\max}\frac{(3h_{\mathrm{go}} - h_{\mathrm{stop}} - 2h)(h - h_{\mathrm{stop}})^2}{(h_{\mathrm{go}} - h_{\mathrm{stop}})^3}\,. \tag{5}$$

In steady state, both vehicles travel at the reference speed, that is, $v^\star_{-1} = v^\star = v_{\mathrm{ref}}$, and the headway is obtained from the inverse of the range policy function: $h^\star_{-1} = V^{-1}(v_{\mathrm{ref}})$.

Let us introduce the shifted coordinates as

$$\tilde{h}_{-1} = h_{-1} - h^\star, \quad \tilde{v}_{-1} = v_{-1} - v^\star_{-1}, \quad \tilde{v} = v - v^\star, \tag{6}$$

while the corresponding state vector assumes the form

$$\mathbf{x} = [\tilde{h}_{-1}\ \tilde{v}_{-1}\ \tilde{v}]^{\mathsf{T}}\,. \tag{7}$$

Then, the equation of motion can be rewritten in the form of the delay differential equation (DDE):

$$\dot{\mathbf{x}}(t) = \mathbf{L}\mathbf{x}(t) + \mathbf{R}\mathbf{x}(t-\tau) + \mathbf{N}(\mathbf{x}(t-\tau))\,, \tag{8}$$

with

$$\mathbf{L} = \begin{bmatrix} 0 & -1 & 1 \\ 0 & 0 & 0 \\ 0 & 0 & 0 \end{bmatrix},\ \mathbf{R} = \begin{bmatrix} 0 & 0 & 0 \\ \alpha\kappa & -\alpha-\beta & \beta \\ 0 & \beta_{-1} & -\hat{\beta}-\beta_{-1} \end{bmatrix}, \tag{9}$$

where κ is the slope of the range policy function at $h_{-1} = h^\star_{-1}$; see Fig. 1(b). Furthermore, the Taylor expansion of the nonlinearity assumes the form

$$\mathbf{N}(\mathbf{\Phi}) = \frac{1}{2}\mathbf{g}_2(\mathbf{\Phi},\mathbf{\Phi}) + \frac{1}{6}\mathbf{g}_3(\mathbf{\Phi},\mathbf{\Phi},\mathbf{\Phi}) \tag{10}$$

with

$$\mathbf{g}_2(\mathbf{\Phi}(-\tau),\mathbf{\Psi}(-\tau)) = \begin{bmatrix} 0 \\ \alpha V''(h^\star_{-1})\Phi_1(-\tau)\Psi_1(-\tau) \\ 0 \end{bmatrix}, \tag{11}$$

$$\begin{aligned}&\mathbf{g}_3(\mathbf{\Phi}(-\tau),\mathbf{\Psi}(-\tau),\mathbf{\Lambda}(-\tau)) = \\ &= \begin{bmatrix} 0 \\ \alpha V'''(h^\star_{-1})\Phi_1(-\tau)\Psi_1(-\tau)\Lambda_1(-\tau) \\ 0 \end{bmatrix}.\end{aligned} \tag{12}$$

Here, prime denotes the differentiation with respect to the headway, while the subscript 1 refers to the first component of the 3-dimensional vectors $\mathbf{\Phi}$, $\mathbf{\Psi}$, and $\mathbf{\Lambda}$.

The corresponding characteristic matrix is

$$\mathbf{\Delta}(\lambda) = \lambda\mathbf{I} - \mathbf{L} - \mathbf{R}\mathrm{e}^{-\lambda\tau}\,, \tag{13}$$

the determinant of which yields the characteristic equation

$$\begin{aligned}&\lambda^3 + ((\alpha+\beta+\hat{\beta}+\beta_{-1})\lambda^2 + \alpha\kappa\lambda)\mathrm{e}^{-\lambda\tau} \\ &\quad + ((\beta\hat{\beta} + \alpha\hat{\beta} + \alpha\beta_{-1})\lambda + \alpha\kappa\hat{\beta})\mathrm{e}^{-2\lambda\tau} = 0\,.\end{aligned} \tag{14}$$

The linear stability analysis is carried out in detail in Szaksz et al. (2023).

3. SPECTRAL SUBMANIFOLD CALCULATION

Although, the characteristic equation (14) has got infinitely many roots, only finite number of them are located to the right of a vertical line in the complex plane (Hale and Verduyn Lunel, 2013; Stepan, 1989). This allows one to project the dynamics to a selected finite dimensional subspace. In this section, we combine the concept of spectral submanifolds (Haller and Ponsioen, 2016) with the dual perturbation framework (Diekmann et al., 1995) to obtain reduced-order models of the original system (8).

Let us define the state vector

$$\mathbf{x}_t(\vartheta) = \mathbf{x}(t+\vartheta)\,,\ \vartheta \in [-\tau, 0], \tag{15}$$

in the Banach space $\mathcal{B} = \mathcal{C}([-\tau,0],\mathbb{C}^3)$, with the help of which the DDE (8) can be written in the form of the operator differential equation (OpDE):

$$\dot{\mathbf{x}}_t(\vartheta) = \mathcal{A}^{\odot\star}\mathbf{x}_t(\vartheta) + \mathcal{N}(\mathbf{x}_t(\vartheta)). \tag{16}$$

Here, the linear operator $\mathcal{A}^{\odot\star} : \mathcal{B} \to \mathcal{B}$ and the nonlinear operator $\mathcal{N} : \mathcal{B} \to \mathcal{B}$ assume the form

$$\mathcal{A}^{\odot\star}\mathbf{\Phi} = \begin{cases} \frac{\mathrm{d}\mathbf{\Phi}}{\mathrm{d}\vartheta}(\vartheta)\,, & \text{if } \vartheta \in [-\tau, 0)\,, \\ \mathbf{L}\mathbf{\Phi}(0) + \mathbf{R}\mathbf{\Phi}(-\tau)\,, & \text{if } \vartheta = 0\,, \end{cases} \tag{17}$$

$$\mathcal{N}(\mathbf{\Phi}) = \begin{cases} \mathbf{0}\,, & \text{if } \vartheta \in [-\tau, 0)\,, \\ \mathbf{N}(\mathbf{\Phi}(-\tau))\,, & \text{if } \vartheta = 0\,, \end{cases} \tag{18}$$

respectively. Note that $\star$ (star) denotes the adjoint, while $\odot$ (sun) denotes the adjoint in a restricted domain to be defined later. Similar to the Hopf bifurcation analysis in the book of Kuznetsov (1998), the nonlinear operator can be separated into second and third order terms:

$$\mathcal{N}(\mathbf{\Phi}) = \frac{1}{2!}\mathbf{B}(\mathbf{\Phi},\mathbf{\Phi}) + \frac{1}{3!}\mathbf{C}(\mathbf{\Phi},\mathbf{\Phi},\mathbf{\Phi})\,, \tag{19}$$

where

$$\mathbf{B}(\mathbf{\Phi},\mathbf{\Psi}) = \begin{cases} \mathbf{0}\,, & \text{if } \vartheta \in [-\tau, 0), \\ \mathbf{g}_2(\mathbf{\Phi}(-\tau),\mathbf{\Psi}(-\tau)), & \text{if } \vartheta = 0\,, \end{cases} \tag{20}$$

$$\mathbf{C}(\mathbf{\Phi},\mathbf{\Psi},\mathbf{\Lambda}) = \begin{cases} \mathbf{0}\,, & \text{if } \vartheta \in [-\tau, 0), \\ \mathbf{g}_3(\mathbf{\Phi}(-\tau),\mathbf{\Psi}(-\tau),\mathbf{\Lambda}(-\tau)), & \text{if } \vartheta = 0\,. \end{cases} \tag{21}$$

To obtain the dynamics on a spectral submanifold, one needs the eigenfunctions of the operator $\mathcal{A}^{\odot\star}$ corresponding to the selected eigenvalues. The eigenfunction $\mathbf{s} \in \mathcal{B}$ corresponding to a dominant eigenvalue λ satisfies

$$\mathcal{A}^{\odot\star}\mathbf{s} = \lambda\mathbf{s}\,. \tag{22}$$

The solution of the corresponding boundary value problem (BVP) assumes the form

$$\mathbf{s}(\vartheta) = \mathbf{q}\mathrm{e}^{\lambda\vartheta}\,, \tag{23}$$

where $\mathbf{q} \in \mathbb{C}^3$ spans the null space of the characteristic matrix $\mathbf{\Delta}(\lambda)$:

$$\mathbf{\Delta}(\lambda)\mathbf{q} = \mathbf{0}\,. \tag{24}$$

Note that the null space can be determined up to a free scalar multiplier; let us select the first component of $\mathbf{q}$ as 1 meter, which yields:

$$\mathbf{q} = \begin{bmatrix} 1 \\ -\frac{\lambda^2+\lambda(\hat{\beta}+\beta_{-1})\mathrm{e}^{-\lambda\tau}}{\lambda+\hat{\beta}\mathrm{e}^{-\lambda\tau}} \\ -\frac{\lambda\beta_{-1}\mathrm{e}^{-\lambda\tau}}{\lambda+\hat{\beta}\mathrm{e}^{-\lambda\tau}} \end{bmatrix}. \tag{25}$$

To project the dynamics onto a particular spectral subspace, let us introduce the adjoint operator $\mathcal{A}^{\odot}$ in the form

$$\mathcal{A}^{\odot}\mathbf{\Psi} = \begin{cases} \frac{\mathrm{d}\mathbf{\Psi}}{\mathrm{d}\sigma}(0)\,, & \text{if } \sigma = 0\,, \\ \frac{\mathrm{d}\mathbf{\Psi}}{\mathrm{d}\sigma}(\sigma) + \mathbf{\Psi}(0)\mathbf{L}\,, & \text{if } \sigma \in (0,\tau)\,, \\ \mathbf{\Psi}(0)(\mathbf{L}+\mathbf{R})\,, & \text{if } \sigma = \tau\,, \end{cases} \tag{26}$$

where $\mathbf{\Psi} \in \mathcal{B}^{\star} = \mathcal{C}([0,\tau],\mathbb{C}^3)$, while $\mathbf{\Psi}(0)$ is a row vector. The operator $\mathcal{A}^{\odot}$ acts on the restricted domain

$$\mathcal{D}(\mathcal{A}^{\odot}) = \left\{ \mathbf{\Psi} \in \mathcal{B}^{\star} : \frac{\mathrm{d}\mathbf{\Psi}}{\mathrm{d}\sigma}(\tau) = \mathbf{0} \right\}. \tag{27}$$

Then, the operators $\mathcal{A}^{\odot}$ and $\mathcal{A}^{\odot\star}$ are adjoint to each other:

$$\langle \mathcal{A}^{\odot}\mathbf{\Psi}, \mathbf{\Phi}\rangle = \langle \mathbf{\Psi}, \mathcal{A}^{\odot\star}\mathbf{\Phi}\rangle\,, \tag{28}$$

where $\langle .,. \rangle$ denotes the pairing

$$\langle \mathbf{\Psi}, \mathbf{\Phi}\rangle = \mathbf{\Psi}(0)\mathbf{\Phi}(0) + \int_0^{\tau} \frac{\mathrm{d}\mathbf{\Psi}}{\mathrm{d}\theta}(\theta)\mathbf{\Phi}(-\theta)\mathrm{d}\theta\,. \tag{29}$$

The spectrum of the operators $\mathcal{A}^{\odot\star}$ and $\mathcal{A}^{\odot}$ are the same, that is, the eigenfunction of $\mathcal{A}^{\odot}$ corresponding the dominant eigenvalue λ satisfies

$$\mathcal{A}^{\odot}\mathbf{n} = \lambda\mathbf{n}\,. \tag{30}$$

The solution of this BVP leads to

$$\mathbf{n}(\sigma) = \begin{cases} \mathbf{p}\mathrm{e}^{\lambda\sigma}\,, & \text{if } \sigma \le 0\,, \\ \mathbf{p}\left(\mathbf{I} + \mathbf{R}\mathrm{e}^{-\lambda\tau}\frac{\mathrm{e}^{\lambda\sigma}-1}{\lambda}\right), & \text{if } \sigma \in (0,\tau)\,, \\ \mathbf{p}\left(\mathbf{I} + \mathbf{R}\mathrm{e}^{-\lambda\tau}\frac{\mathrm{e}^{\lambda\tau}-1}{\lambda}\right), & \text{if } \sigma \ge \tau\,, \end{cases} \tag{31}$$

with continuous extension at $\lambda = 0$. Here, the row vector $\mathbf{p} \in \mathbb{C}^3$ spans the left nullspace of the characteristic matrix $\mathbf{\Delta}(\lambda)$, that is, it satisfies the equation

$$\mathbf{p}\mathbf{\Delta}(\lambda) = \mathbf{0}\,. \tag{32}$$

Let us choose the second coordinate of $\mathbf{p}$ as the free variable, which yields

$$\mathbf{p} = \left[\frac{\alpha\kappa\mathrm{e}^{-\lambda\tau}}{\lambda}p_2 \quad p_2 \quad \frac{(\alpha\kappa+\lambda\beta)\mathrm{e}^{-\lambda\tau}}{\lambda^2+\lambda(\hat{\beta}+\beta_{-1})\mathrm{e}^{-\lambda\tau}}p_2\right], \tag{33}$$

while the variable p_2 is restricted by the normalization

$$\langle \mathbf{n}, \mathbf{s}\rangle = 1\,. \tag{34}$$

After some algebraic manipulation, the normalization assumes the form

$$\mathbf{p}\mathbf{\Delta}'(\lambda)\mathbf{q} = 1\,, \tag{35}$$

where, prime denotes the derivative with respect to λ. This yields a lengthy expression for p_2, which is not presented here.

Finally, the projection of a solution $\mathbf{x}_t$ to the eigenfunction $\mathbf{s}$ is obtained by pairing the solution with $\mathbf{n}$, which leads to the spectral coordinate

$$y(t) = \mathbf{p}\left(\mathbf{x}(t) + \int_{-\tau}^{0} \mathbf{R}\mathrm{e}^{-\lambda(\vartheta+\tau)}\mathbf{x}(t+\vartheta)\mathrm{d}\vartheta\right). \tag{36}$$

In the following, the spectral submanifold and the corresponding reduced dynamics are obtained for two particular control gain combinations of the AV. The first case leads to a real dominant eigenvalue, while in the second case, the dominant eigenvalues form a complex conjugate pair.

3.1 Projection to the manifold corresponding to a dominant real eigenvalue

Assume that λ_1 denotes the real dominant eigenvalue of the linearized system. Then, the corresponding spectral submanifold can be searched in the form

$$\mathbf{W}(z;\vartheta) = \mathbf{W}_1(\vartheta)z + \frac{1}{2}\mathbf{W}_2(\vartheta)z^2 + \frac{1}{6}\mathbf{W}_3(\vartheta)z^3 + \mathcal{O}(z^4), \tag{37}$$

with the parametrization variable z, while the dynamics on the SSM is governed by the nonlinear differential equation

$$\dot{z} = \lambda_1 z + \beta_2 z^2 + \beta_3 z^3\,. \tag{38}$$

Considering the relevant dynamics $\mathbf{x}_t(\vartheta) = \mathbf{W}(z(t);\vartheta)$, the OpDE (16) results the homological equation

$$\frac{\partial \mathbf{W}(z;\vartheta)}{\partial z}\dot{z} = \mathcal{A}^{\odot\star}\mathbf{W}(z;\vartheta) + \mathcal{N}(\mathbf{W}(z;\vartheta))\,. \tag{39}$$

After the substitution of (37) and (38) into (39), calculate the polynomial balance in z, which yields the BVPs

$$\lambda_1\mathbf{W}_1 = \mathcal{A}^{\odot\star}\mathbf{W}_1\,, \tag{40}$$

$$(2\lambda_1\mathcal{I} - \mathcal{A}^{\odot\star})\mathbf{W}_2 = \mathbf{B}(\mathbf{W}_1,\mathbf{W}_1) - 2\beta_2\mathbf{W}_1\,, \tag{41}$$

$$\begin{aligned}(3\lambda_1\mathcal{I} - \mathcal{A}^{\odot\star})\mathbf{W}_3 &= 3\mathbf{B}(\mathbf{W}_1,\mathbf{W}_2) \\ &+ \mathbf{C}(\mathbf{W}_1,\mathbf{W}_1,\mathbf{W}_1) - 6\beta_2\mathbf{W}_2 - 6\beta_3\mathbf{W}_1\,.\end{aligned} \tag{42}$$

Equation (40) implies that $\mathbf{W}_1$ is the eigenfunction of the operator $\mathcal{A}^{\odot\star}$ corresponding to the eigenvalue λ_1, that is,

$$\mathbf{W}_1(\vartheta) = \mathbf{q}\mathrm{e}^{\lambda_1\vartheta}\,. \tag{43}$$

Due to the selection of the reduced dynamics (38), we have

$$\langle \mathbf{n}, \mathbf{W}_2\rangle = 0\,, \quad \text{and} \quad \langle \mathbf{n}, \mathbf{W}_3\rangle = 0\,. \tag{44}$$

Then, pairing $\mathbf{n}$ with (41), (42) results the coefficients

$$\beta_2 = \frac{1}{2}\mathbf{p}\mathbf{g}_2(\mathbf{s}(-\tau),\mathbf{s}(-\tau))\,, \tag{45}$$

$$\beta_3 = \frac{1}{6}\mathbf{p}[3\mathbf{g}_2(\mathbf{s}(-\tau),\mathbf{W}_2(-\tau)) + \mathbf{g}_3(\mathbf{s}(-\tau),\mathbf{s}(-\tau),\mathbf{s}(-\tau))]\,, \tag{46}$$

where $\mathbf{s}(-\tau) = \mathbf{q}\mathrm{e}^{-\lambda_1\tau}$; see (23). Finally, considering the non-resonance conditions

$$\mathrm{Ker}(k\lambda_1\mathcal{I} - \mathcal{A}^{\odot\star}) \neq \{0\}, \quad k = 2,3\,, \tag{47}$$

the solutions of the BVPs (41), (42) yield:

$$\begin{aligned}\mathbf{W}_2(\vartheta) &= \mathbf{\Delta}^{-1}(2\lambda_1)\mathbf{g}_2(\mathbf{s}(-\tau),\mathbf{s}(-\tau))\mathrm{e}^{2\lambda_1\vartheta} \\ &- 2\frac{\beta_2}{\lambda_1}\mathbf{q}\mathrm{e}^{\lambda_1\vartheta}\,,\end{aligned} \tag{48}$$

$$\begin{aligned}\mathbf{W}_3(\vartheta) &= \mathbf{\Delta}^{-1}(3\lambda_1)[3\mathbf{g}_2(\mathbf{s}(-\tau),\mathbf{W}_2(-\tau)) \\ &+ \mathbf{g}_3(\mathbf{s}(-\tau),\mathbf{s}(-\tau),\mathbf{s}(-\tau))]\mathrm{e}^{3\lambda_1\vartheta} \\ &+ 6\frac{\beta_2}{\lambda_1}\mathbf{\Delta}^{-1}(3\lambda_1)\mathbf{g}_2(\mathbf{s}(-\tau),\mathbf{s}(-\tau))\mathrm{e}^{3\lambda_1\vartheta} \\ &- 6\frac{\beta_2}{\lambda_1}\mathbf{g}_2(\mathbf{s}(-\tau),\mathbf{s}(-\tau))\mathrm{e}^{2\lambda_1\vartheta} \\ &+ \left(6\frac{\beta_3^2}{\lambda_1^2} - 3\frac{\beta_3}{\lambda_1}\right)\mathbf{q}\mathrm{e}^{\lambda_1\vartheta}\,.\end{aligned} \tag{49}$$

The expansions of the above expressions are lengthy, hence, we discuss a numerical example. Let us fix the delay to $\tau = 0.4\,\mathrm{s}$, while the further parameters

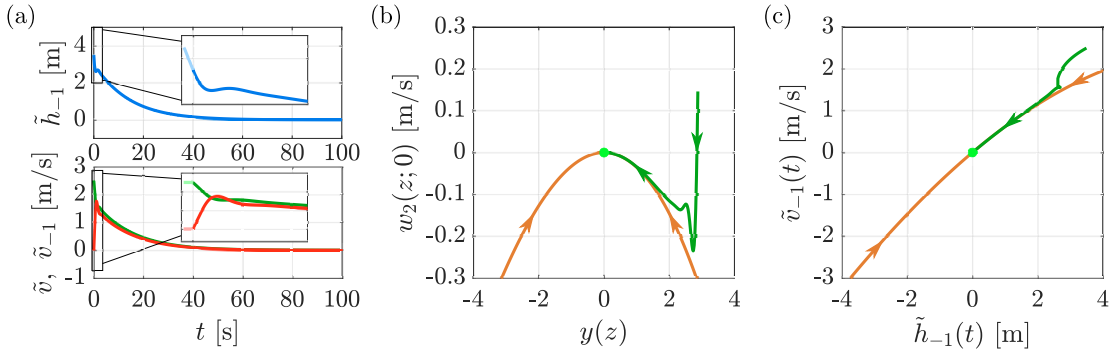

Fig. 2. Convergence of a particular trajectory towards the spectral submanifold corresponding to a dominant real root. Panel (a) presents the headway and the vehicle velocity signals corresponding to the initial conditions $\tilde{v}_{-1}(t) \equiv 2.5\,\mathrm{m/s}$, $\tilde{v}(t) \equiv 0\,\mathrm{m/s}$, $\tilde{h}_{-1}(0) = 3.5\,\mathrm{m}$, and $\tilde{h}_{-1}(t) = \tilde{h}_{-1}(0) - \tilde{v}_{-1}(0)t$ for $t \in [-\tau, 0]$. The blue curve refers to the evolution of the headway, while the green and red curves refer to the velocity of the HV and AV, respectively. Panel (b) shows the second coordinate of the trajectory (green) and that of the SSM (brown) above the space of the dominant eigenvector. Panel (c) displays the velocity of the HV as a function of its headway (green) and the corresponding SSM (brown).

are $\hat{\beta} = 0.2\,\mathrm{s}^{-1}$, $\beta_{-1} = 1\,\mathrm{s}^{-1}$, $\alpha = 0.3\,\mathrm{s}^{-1}$, $\beta = 0.4\,\mathrm{s}^{-1}$, $v_{\max} = 30\,\mathrm{m/s}$, $v_{\mathrm{ref}} = 26.55\,\mathrm{m/s}$, $h_{\mathrm{go}} = 55\,\mathrm{m}$, $h_{\mathrm{stop}} = 5\,\mathrm{m}$. In this case, the dominant eigenvalue has the numerical value $\lambda_1 = -0.0746\,\mathrm{s}^{-1}$, which is well separated from the second rightmost eigenvalue $\lambda_2 = -0.3610\,\mathrm{s}^{-1}$.

Then, the vectors $\mathbf{q}$ and $\mathbf{p}$ take the form

$$\mathbf{q} = \begin{bmatrix} 1 \\ 0.6593 \\ 0.5847 \end{bmatrix}, \quad \mathbf{p} = [0.8697, \ -0.3501, \ 0.6244], \tag{50}$$

respectively. Note that here and in the following calculations, the coordinates are obtained in SI units, which are not denoted for the sake of brevity.

Furthermore, for this parameter setting, (43)-(49) yield

$$\mathbf{W}_1(\vartheta) = \begin{bmatrix} \mathrm{e}^{\lambda_1\vartheta} \\ 0.6595\,\mathrm{e}^{\lambda_1\vartheta} \\ 0.5849\,\mathrm{e}^{\lambda_1\vartheta} \end{bmatrix}, \tag{51}$$

$$\mathbf{W}_2(\vartheta) = \begin{bmatrix} 0.0621\,\mathrm{e}^{\lambda_1\vartheta} - 0.0410\,\mathrm{e}^{2\lambda_1\vartheta} \\ 0.0410\,\mathrm{e}^{\lambda_1\vartheta} - 0.1092\,\mathrm{e}^{2\lambda_1\vartheta} \\ 0.0363\,\mathrm{e}^{\lambda_1\vartheta} - 0.1031\,\mathrm{e}^{2\lambda_1\vartheta} \end{bmatrix}, \tag{52}$$

$$\mathbf{W}_3(\vartheta) = \begin{bmatrix} 0.0099\,\mathrm{e}^{\lambda_1\vartheta} - 0.0076\,\mathrm{e}^{2\lambda_1\vartheta} - 0.0001\,\mathrm{e}^{3\lambda_1\vartheta} \\ 0.0065\,\mathrm{e}^{\lambda_1\vartheta} - 0.0204\,\mathrm{e}^{2\lambda_1\vartheta} + 0.0069\,\mathrm{e}^{3\lambda_1\vartheta} \\ 0.0058\,\mathrm{e}^{\lambda_1\vartheta} - 0.0192\,\mathrm{e}^{2\lambda_1\vartheta} + 0.0069\,\mathrm{e}^{3\lambda_1\vartheta} \end{bmatrix}, \tag{53}$$

and

$$\beta_2 = 2.3176 \cdot 10^{-3}, \quad \beta_3 = 0.1011 \cdot 10^{-3}. \tag{54}$$

The corresponding infinite dimensional SSM is obtained from (37); fixing $\vartheta = 0$, the SSM takes the form

$$\mathbf{W}(z;0) = \begin{bmatrix} 1.0000 \\ 0.6595 \\ 0.5849 \end{bmatrix} z + \begin{bmatrix} -0.0211 \\ -0.0682 \\ -0.0668 \end{bmatrix} z^2 + \begin{bmatrix} 0.0021 \\ -0.0069 \\ -0.0065 \end{bmatrix} z^3, \tag{55}$$

while the dynamics on the manifold is governed by

$$\dot{z} = -0.0746z + 0.0023z^2 + 0.0001z^3. \tag{56}$$

Finally, pairing the eigenfunction $\mathbf{n}$ with the manifold $\mathbf{W}$ yields the coordinate along the eigenfunction $\mathbf{s}$:

$$y(z) = \langle \mathbf{n}, \mathbf{W}(z) \rangle = z. \tag{57}$$

Thus, that part of the spectral submanifold, which is orthogonal to $\mathbf{s}$, takes the form

$$\mathbf{w}(z;\vartheta) = \mathbf{W}(z;\vartheta) - y(z)\mathbf{s}(\vartheta), \tag{58}$$

which implies

$$\mathbf{w}(z;0) = \begin{bmatrix} -0.0211 \\ -0.0682 \\ -0.0668 \end{bmatrix} z^2 + \begin{bmatrix} 0.0021 \\ -0.0069 \\ -0.0065 \end{bmatrix} z^3. \tag{59}$$

Figure 2 presents the convergence of a particular trajectory towards the SSM. Panel (a) displays the time evolution of the solution corresponding to the given initial condition. Panel (b) presents the second coordinate of $\mathbf{w}(z;0)$ and that of the trajectory above the space spanned by the dominant eigenvector, while panel (c) displays the velocity of the HV as a function of its headway. Clearly, the trajectory quickly approaches the SSM and approaches the stable fixed point along that. That is the SSM provides a good approximation of the dominant dynamics.

3.2 Projection to the manifold corresponding to a pair of complex conjugate eigenvalues

Varying the system parameters, the dominant eigenvalues may form a complex conjugate pair: λ_1 and $\lambda_2 = \overline{\lambda}_1$. Then, the SSM can be represented in the form

$$\begin{aligned} \mathbf{W}(z,\overline{z};\vartheta) &= \mathbf{W}_{10}(\vartheta)z + \mathbf{W}_{01}(\vartheta)\overline{z} \\ &+ \frac{1}{2}\mathbf{W}_{20}(\vartheta)z^2 + \mathbf{W}_{11}(\vartheta)z\overline{z} + \frac{1}{2}\mathbf{W}_{02}(\vartheta)\overline{z}^2 \\ &+ \frac{1}{6}\mathbf{W}_{30}(\vartheta)z^3 + \frac{1}{2}\mathbf{W}_{21}(\vartheta)z^2\overline{z} \\ &+ \frac{1}{2}\mathbf{W}_{12}(\vartheta)z\overline{z}^2 + \frac{1}{6}\mathbf{W}_{03}(\vartheta)\overline{z}^3 + \mathcal{O}\big(|z|^4\big), \end{aligned} \tag{60}$$

while the reduced dynamics is governed by the normal form

$$\begin{bmatrix} \dot{z} \\ \dot{\overline{z}} \end{bmatrix} = \begin{bmatrix} \lambda_1 z + \beta_{21} z^2\overline{z} \\ \overline{\lambda}_1\overline{z} + \overline{\beta}_{21} z\overline{z}^2 \end{bmatrix}. \tag{61}$$

Balancing the terms of the corresponding homological equation

$$\begin{aligned} &\frac{\partial \mathbf{W}(z,\overline{z};\vartheta)}{\partial z}\dot{z} + \frac{\partial \mathbf{W}(z,\overline{z};\vartheta)}{\partial \overline{z}}\dot{\overline{z}} \\ &= \mathcal{A}^{\odot\star}\mathbf{W}(z,\overline{z};\vartheta) + \mathcal{N}(\mathbf{W}(z,\overline{z};\vartheta)), \end{aligned} \tag{62}$$

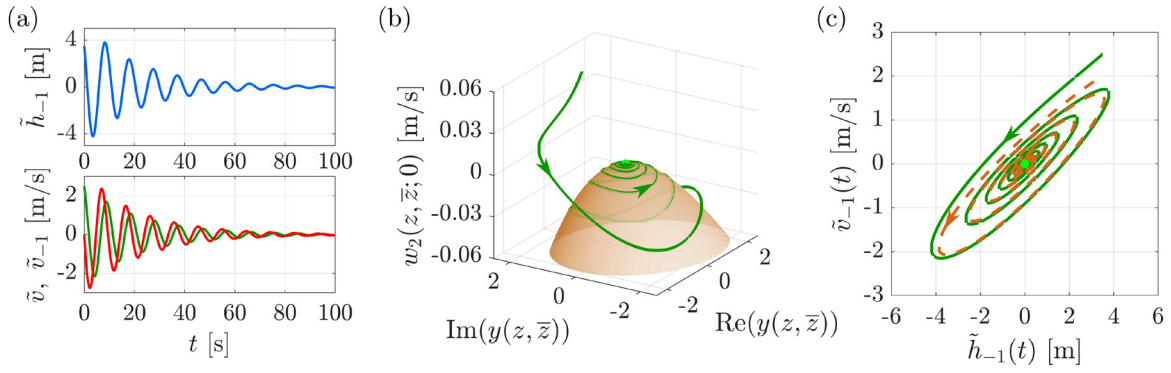

Fig. 3. Convergence of a particular trajectory towards the SSM corresponding to the dominant pair of complex conjugate roots. Panel (a) presents the headway and the vehicle velocity signals corresponding to the initial conditions $\tilde{v}_{-1}(t) \equiv 2.5\,\mathrm{m/s}$, $\tilde{v}(t) \equiv 0\,\mathrm{m/s}$, $\tilde{h}_{-1}(0) = 3.5\,\mathrm{m}$, and $\tilde{h}_{-1}(t) = \tilde{h}_{-1}(0) - \tilde{v}_{-1}(0)t$ for $t \in [-\tau, 0]$. The blue curve refers to the evolution of the headway, while the green and red curves refer to the velocity of the HV and AV, respectively. Panel (b) shows the second coordinate of the trajectory (green curve) and that of the SSM (brown surface) above the space of the real and imaginary part of the dominant eigenvector. Panel (c) displays the velocity of the HV as a function of its headway (green) and the corresponding reduced dynamics based trajectory (brown).

one obtains that

$$\mathbf{W}_{10}(\vartheta) = \mathbf{s}(\vartheta)\,, \quad \text{and} \quad \mathbf{W}_{01}(\vartheta) = \bar{\mathbf{s}}(\vartheta)\,, \tag{63}$$

while the further coefficients satisfy the BVPs

$$(2\lambda_1\mathcal{I} - \mathcal{A}^{\odot\star})\mathbf{W}_{20} = \mathbf{B}(\mathbf{s},\mathbf{s})\,, \tag{64}$$

$$((\lambda_1+\overline{\lambda}_1)\mathcal{I} - \mathcal{A}^{\odot\star})\mathbf{W}_{11} = \mathbf{B}(\mathbf{s},\bar{\mathbf{s}})\,, \tag{65}$$

$$(3\lambda_1\mathcal{I} - \mathcal{A}^{\odot\star})\mathbf{W}_{30} = 3\mathbf{B}(\mathbf{s},\mathbf{W}_{20}) + \mathbf{C}(\mathbf{s},\mathbf{s},\mathbf{s})\,, \tag{66}$$

$$\begin{aligned}((2\lambda_1+\overline{\lambda}_1)\mathcal{I} - \mathcal{A}^{\odot\star})\mathbf{W}_{21} &= 2\mathbf{B}(\mathbf{s},\mathbf{W}_{11}) + \mathbf{B}(\bar{\mathbf{s}},\mathbf{W}_{20}) \\ &\quad + \mathbf{C}(\bar{\mathbf{s}},\mathbf{s},\mathbf{s}) - 2\beta_{21}\mathbf{s}\,,\end{aligned} \tag{67}$$

where we utilized (63).

According to the selection of the normal form (61), we have $\langle \mathbf{n}, \mathbf{W}_{21}\rangle = 0$. Then, under the non-resonance conditions

$$\mathrm{Ker}((k\lambda_1 + l\lambda_2)\mathcal{I} - \mathcal{A}^{\odot\star}) \neq \{0\}, \quad k+l = 2,3\,. \tag{68}$$

the solution of (64)-(67) leads to the expressions

$$\mathbf{W}_{20}(\vartheta) = \mathbf{\Delta}^{-1}(2\lambda_1)\mathbf{g}_2(\mathbf{s}(-\tau),\mathbf{s}(-\tau))\mathrm{e}^{2\lambda_1\vartheta}, \tag{69}$$

$$\mathbf{W}_{11}(\vartheta) = \mathbf{\Delta}^{-1}(\lambda_1+\overline{\lambda}_1)\mathbf{g}_2(\mathbf{s}(-\tau),\bar{\mathbf{s}}(-\tau))\mathrm{e}^{(\lambda_1+\overline{\lambda}_1)\vartheta}, \tag{70}$$

$$\begin{aligned}\mathbf{W}_{30}(\vartheta) &= \mathbf{\Delta}^{-1}(3\lambda_1)[3\mathbf{g}_2(\mathbf{s}(-\tau),\mathbf{W}_{20}(-\tau)) \\ &\quad + \mathbf{g}_3(\mathbf{s}(-\tau),\mathbf{s}(-\tau),\mathbf{s}(-\tau))]\mathrm{e}^{3\lambda_1\vartheta},\end{aligned} \tag{71}$$

$$\begin{aligned}\mathbf{W}_{21}(\vartheta) &= \mathbf{\Delta}^{-1}(2\lambda_1+\overline{\lambda}_1)[\mathbf{g}_2(\bar{\mathbf{s}}(-\tau),\mathbf{W}_{20}(-\tau)) \\ &\quad + 2\mathbf{g}_2(\mathbf{s}(-\tau),\mathbf{W}_{11}(-\tau)) \\ &\quad + \mathbf{g}_3(\bar{\mathbf{s}}(-\tau),\mathbf{s}(-\tau),\mathbf{s}(-\tau))]\mathrm{e}^{(2\lambda_1+\overline{\lambda}_1)\vartheta} \\ &\quad - \frac{2\beta_{21}}{\lambda_1+\overline{\lambda}_1}\mathbf{q}\mathrm{e}^{\lambda\vartheta},\end{aligned} \tag{72}$$

while

$$\begin{aligned}\beta_{21} = \frac{1}{2}\mathbf{p}[&\mathbf{g}_2(\bar{\mathbf{s}}(-\tau),\mathbf{W}_{20}(-\tau)) + 2\mathbf{g}_2(\mathbf{s}(-\tau),\mathbf{W}_{11}(-\tau)) \\ &+ \mathbf{g}_3(\bar{\mathbf{s}}(-\tau),\mathbf{s}(-\tau),\mathbf{s}(-\tau))]\,.\end{aligned} \tag{73}$$

The coefficients form complex conjugate pairs, thus

$$\mathbf{W}_{02} = \overline{\mathbf{W}}_{20}\,, \quad \mathbf{W}_{03} = \overline{\mathbf{W}}_{30}\,, \quad \mathbf{W}_{12} = \overline{\mathbf{W}}_{21}\,. \tag{74}$$

Let us fix the parameters to the same values as in the previous subsection, except for the control gains of the AV, which are now set at $\hat{\beta} = 0.8\,\mathrm{s}^{-1}$ and $\beta_{-1} = -0.8\,\mathrm{s}^{-1}$. This yields that the dominant eigenvalues form the complex conjugate pair:

$$\lambda_{1,2} = -0.0439 \pm 0.6559\,\mathrm{i}\,, \tag{75}$$

while the vectors $\mathbf{q}$ and $\mathbf{p}$ take the forms

$$\mathbf{q} = \begin{bmatrix} 1 \\ 0.4586 - 0.1972\,\mathrm{i} \\ 0.4148 + 0.4587\,\mathrm{i}\end{bmatrix}, \qquad \mathbf{p} = \begin{bmatrix}0.1935 - 0.2316\,\mathrm{i} \\ 0.5622 + 0.9261\,\mathrm{i} \\ 0.0591 - 0.7851\,\mathrm{i}\end{bmatrix}^{\mathsf{T}}. \tag{76}$$

In this case, the ϑ-dependent coefficients of the SSM lead to lengthy expressions, therefore, we present only their headpoints at $\vartheta = 0$:

$$\mathbf{W}_{20}(0) = \begin{bmatrix}-0.0051 + 0.0086\,\mathrm{i} \\ 0.0045 + 0.0151\,\mathrm{i} \\ -0.0063 + 0.0076\,\mathrm{i}\end{bmatrix}, \tag{77}$$

$$\mathbf{W}_{11}(0) = \begin{bmatrix}0.0848 \\ -0.0009 \\ -0.0083\end{bmatrix}, \tag{78}$$

$$\mathbf{W}_{30}(0) = \begin{bmatrix}-0.1546 + 0.1312\,\mathrm{i} \\ 0.1315 + 0.5289\,\mathrm{i} \\ -0.1062 + 0.2074\,\mathrm{i}\end{bmatrix} \cdot 10^{-3}, \tag{79}$$

$$\mathbf{W}_{21}(0) = \begin{bmatrix}3.3194 - 4.3679\,\mathrm{i} \\ 0.8610 + 2.3238\,\mathrm{i} \\ 0.9662 + 2.6859\,\mathrm{i}\end{bmatrix} \cdot 10^{-3}. \tag{80}$$

In addition, the coefficient of the resonant term in the reduced dynamics is obtained as

$$\beta_{21} = (-1.1614 - 1.1949\,\mathrm{i}) \cdot 10^{-3}. \tag{81}$$

Finally, let $y(z,\bar{z}) = \langle \mathbf{n}, \mathbf{W}(z,\bar{z})\rangle$ denote the complex coordinate along the eigenfunction $\mathbf{s}$, which yields the near identity transformation

$$\begin{aligned}y(z,\bar{z}) = z &+ \frac{1}{2}\langle \mathbf{n},\mathbf{W}_{20}\rangle z^2 + \langle \mathbf{n},\mathbf{W}_{11}\rangle z\bar{z} + \frac{1}{2}\langle \mathbf{n},\mathbf{W}_{02}\rangle \bar{z}^2 \\ &+ \frac{1}{6}\langle \mathbf{n},\mathbf{W}_{30}\rangle z^3 + \frac{1}{2}\langle \mathbf{n},\mathbf{W}_{12}\rangle z\bar{z}^2 + \frac{1}{6}\langle \mathbf{n},\mathbf{W}_{03}\rangle \bar{z}^3 + \mathcal{O}\big(|z|^4\big)\,.\end{aligned} \tag{82}$$

Accordingly, the part of the SSM, which is orthogonal to the eigenfunctions $\mathbf{s}$ and $\bar{\mathbf{s}}$, takes the form

$$\mathbf{w}(z,\bar{z};\vartheta) = \mathbf{W}(z,\bar{z};\vartheta) - y(z,\bar{z})\mathbf{s}(\vartheta) - \overline{y}(z,\bar{z})\bar{\mathbf{s}}(\vartheta). \tag{83}$$

Figure 3 presents the convergence of a particular trajectory towards the SSM corresponding to the above parameter

setup. Panel (a) represents the time evolution of the investigated trajectory, while panel (b) illustrates the second coordinate of the SSM and that of the transformed trajectory above the space spanned by the real and imaginary parts of the dominant eigenvector. The trajectory is indicated with the green curve, while the brown surface refers to the spectral submanifold. Clearly, the trajectory quickly approaches the SSM and spirals towards the stable fixed point on that. Finally, panel (c) presents the velocity of the HV as a function of its headway. The original trajectory is the green curve, while the brown dashed line refers to a trajectory on the SSM, which was calculated based on the reduced dynamics. Note that the initial condition of the reduced dynamics was obtained by projecting the original trajectory onto the SSM. As the diagram illustrates, the SSM calculation provides an excellent prediction for the time evolution of the trajectory.

4. CONCLUSION

The powerful concept of spectral submanifolds was combined with the dual perturbation framework to carry out the model reduction of a car-following model where the relevant time delay is also taken into account. The spectral submanifold and the corresponding reduced dynamics are obtained both for the case of a real dominant eigenvalue and for the case of a pair of complex conjugate dominant eigenvalues. The numerical examples presented that, after fast initial transients, the trajectories approach the slow SSM and tend to the stable fixed point along that. Moreover, the trajectory obtained with the reduced dynamics provides an excellent prediction for the solution of the original nonlinear dynamical system. These obtained reduced models enable us to investigate the essential nonlinear dynamics and also to improve the control design of the AV such that it guides the motion of the HV while taking into account the reaction time of the human driver.

In the future, we plan to generalize the concept of SSM to handle multiple time delays and to analyze the nonlinear dynamics for various control parameter configurations. Furthermore, we also plan to examine the self-excited oscillations by analyzing the reduced dynamics. The dual perturbation framework will be extended to non-autonomous delay differential equations, which allows the investigation of car-following systems with time-varying reference velocity.

ACKNOWLEDGEMENTS

The research reported in this paper has been supported by the Hungarian National Research, Development and Innovation Office (NKFI-KKP-133846).

REFERENCES

Breunung, T. and Haller, G. (2018). Explicit backbone curves from spectral submanifolds of forced-damped nonlinear mechanical systems. *Proceedings of the Royal Society A*, 474(2213), 20180083.

Cenedese, M., Axås, J., Bäuerlein, B., Avila, K., and Haller, G. (2022). Data-driven modeling and prediction of non-linearizable dynamics via spectral submanifolds. *Nature Communications*, 13(1), 872.

Cirillo, G.I., Mauroy, A., Renson, L., Kerschen, G., and Sepulchre, R. (2016). A spectral characterization of nonlinear normal modes. *Journal of Sound and Vibration*, 377, 284–301.

Diekmann, O., Van Gils, S.A., Verduyn Lunel, S.M., and Walther, H.O. (1995). *Delay Equations: Functional-, Complex-, and Nonlinear Analysis*, volume 110. Springer, New York.

Hale, J.K. and Verduyn Lunel, S.M. (2013). *Introduction to Functional Differential Equations*, volume 99. Springer, New York.

Haller, G. and Ponsioen, S. (2016). Nonlinear normal modes and spectral submanifolds: existence, uniqueness and use in model reduction. *Nonlinear Dynamics*, 86, 1493–1534.

Kuznetsov, Y.A. (1998). *Elements of Applied Bifurcation Theory*, volume 112. Springer, New York.

Lentjes, B., Spek, L., Bosschaert, M.M., and Kuznetsov, Y.A. (2023). Periodic center manifolds for DDEs in the light of suns and stars. *Journal of Dynamics and Differential Equations*, 1–44.

Molnar, T.G. and Orosz, G. (2024). Destroying phantom jams with connectivity and automation: Nonlinear dynamics and control of mixed traffic. *Transportation Science*. URL `https://doi.org/10.1287/trsc.2023.0498`.

Opreni, A., Vizzaccaro, A., Touzé, C., and Frangi, A. (2023). High-order direct parametrisation of invariant manifolds for model order reduction of finite element structures: application to generic forcing terms and parametrically excited systems. *Nonlinear Dynamics*, 111(6), 5401–5447.

Rosenberg, R. (1966). On nonlinear vibrations of systems with many degrees of freedom. *Advances in Applied Mechanics*, 9, 155–242.

Shaw, S.W. and Pierre, C. (1993). Normal modes for non-linear vibratory systems. *Journal of Sound and Vibration*, 164(1), 85–124.

Stepan, G. (1989). *Retarded Dynamical Systems: Stability and Characteristic Functions*. Longman Scientific & Technical, New York.

Szaksz, B., Orosz, G., and Stepan, G. (2023). Guided control of a human driver via an automated vehicle. *IFAC-PapersOnLine*, 56(2), 899–904. 22nd IFAC World Congress.

Szaksz, B., Orosz, G., and Stepan, G. (2024). Nonlinear guidance of a human driver via an automated vehicle. In *Proceedings of IUTAM Symposium on Nonlinear Dynamics for Design of Mechanical Systems Across Different Length/Time Scales*. Springer. To appear.

Szalai, R., Ehrhardt, D., and Haller, G. (2017). Nonlinear model identification and spectral submanifolds for multi-degree-of-freedom mechanical vibrations. *Proceedings of the Royal Society A*, 473(2202), 20160759.

Vizzaccaro, A., Shen, Y., Salles, L., Blahoš, J., and Touzé, C. (2021). Direct computation of nonlinear mapping via normal form for reduced-order models of finite element nonlinear structures. *Computer Methods in Applied Mechanics and Engineering*, 384, 113957.

Wage, B. (2014). *Normal Form Computations for Delay Differential Equations in DDE-BIFTOOL*. Master's thesis, Universiteit Utrecht, the Netherlands.